Mobility edge for cold atoms in laser speckle potentials

Dominique Delande[1] and Giuliano Orso[2]

[1] *Laboratoire Kastler Brossel, UPMC-Paris6, ENS, CNRS; 4 Place Jussieu, F-75005 Paris, France*
[2] *Laboratoire Matériaux et Phénomènes Quantiques, Université Paris Diderot-Paris 7 and CNRS, UMR 7162, 75205 Paris Cedex 13, France*

(Dated: Published in Physical Review Letters **113**, 060601 (2014))

Using the transfer matrix method, we numerically compute the precise position of the mobility edge of atoms exposed to a laser speckle potential, and study its dependence vs. the disorder strength and correlation function. Our results deviate significantly from previous theoretical estimates using an approximate self-consistent approach of localization. In particular we find that the position of the mobility edge in blue-detuned speckles is much lower than in the red-detuned counterpart, pointing out the crucial role played by the asymmetric on-site distribution of speckle patterns.

PACS numbers: 03.75.-b, 05.30.Rt, 64.70.Tg, 05.60.Gg

arXiv:1403.3821v2 [cond-mat.quant-gas] 17 Feb 2015

Anderson localization (AL), namely the absence of diffusion of waves in certain disordered media, is a ubiquitous phenomenon originating from the interference of multiple scatterings from random defects [1, 2]. Among others, AL has been reported for light waves in diffusive media [3, 4] or photonic crystals [5, 6], sound waves [7], microwaves [8]. Cold atomic gases do have very appealing properties for studying AL: interference effects can be preserved over a relatively long time, atom-atom interaction effects are small thanks to the absence of Coulomb interaction and can be controlled using e.g. Feshbach resonances. Last, but not least, the spatial and temporal typical scales are convenient for a direct observation of the localization effect, starting from an initially localized wavepacket and monitoring its expansion vs. time.

The dimension of the system is a crucial parameter. In dimension 1 (1D) and 2, AL is the generic scenario and was directly observed on 1D atomic Bose gases [9, 10]. In dimension three (3D) and above, there is a metal-insulator transition at a specific energy $E = E_c$, the so-called mobility edge, separating localized ($E < E_c$) from diffusive ($E > E_c$) states.

The kicked rotor model describing cold atoms exposed to a periodic or quasi-periodic sequence of far-detuned laser pulses can be mapped to an Anderson model in momentum space, making it possible to observe 1D AL in momentum space [11] in 1995. More recently, the 3D Anderson transition has been experimentally observed [12], the critical exponent accurately measured and its universality tested [13].

Experiments [14–16] on 3D AL in configuration space, using laser speckles as a source of disorder for atoms, are less advanced. The reasons are twofold. First the broadband energy distribution of the expanding atoms severely complicates the extraction of the mobility edge from the raw data. Second and most important, a direct comparison with theory remains problematic. To date, there is indeed no *exact* theoretical prediction for the mobility edge of atoms in speckle potentials. The currently available [17–19] estimates are based on an approximate self-consistent theory of localization (SCTL) [20].

The experimentally measured [14] position of the mobility edge in highly anisotropic speckles is unexpectedly high compared to the SCTL results. In Ref. [15], the experimentally measured mobility edge is significantly below the most naive implementation of the SCTL [17]. A modified version of the SCTL [21] improves that agreement, with however a predicted mobility edge below the measured value. In Ref. [16], the authors developed a new experimental scheme to directly measure the mobility edge of atoms. For relatively small disorder, their result is apparently above the average potential value, in contrast with the SCTL theoretical expectations.

Contrary to typical condensed matter systems, the on-site distribution $P(V)$ of the blue-detuned speckles employed in experiments [14–16] is not Gaussian, but follows a Poissonian law [22, 23]:

$$P(V) = \frac{\Theta(V+V_0)}{V_0}\ \exp\left(-\frac{V+V_0}{V_0}\right) \qquad (1)$$

where Θ is the Heaviside function and V_0 is related to the variance by $\langle V^2\rangle = V_0^2$. For convenience, we have shifted the potential by its average value. Red-detuned speckles are described by Eq.(1) under the change $V \to -V$.

In this Letter we use transfer matrix calculations together with the finite-size scaling to pinpoint the precise position of the mobility edge for massive particles in laser speckle potentials. We show that *i)* for blue-detuned speckle, the previous theoretical calculations based on the SCTL significantly overestimate the correct position of the mobility edge; *ii)* the values of E_c for red and blue speckles are completely different due to the asymmetry $P(V) \neq P(-V)$ of the distribution (1), while the current implementations of the SCTL would predict the same value; *iii)* at least for isotropic speckles, the position of the mobility edge depends mainly on the width of the correlation function $\langle V(0)V(\mathbf{r})\rangle$ of the potential rather than on its specific shape.

The transfer-matrix approach was first used to study the 3D Anderson model [24, 25]. Its application to

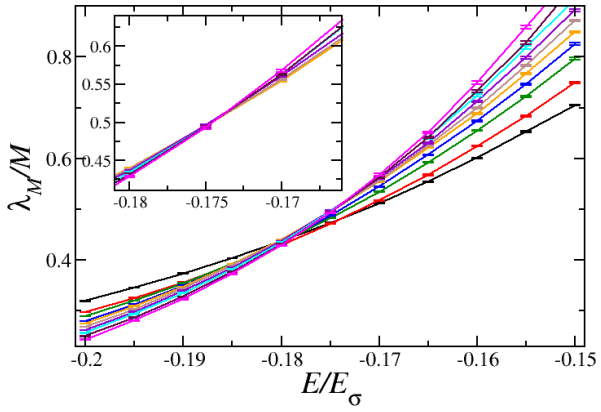

FIG. 1: (color online) Numerical determination of the mobility edge of a cold atom in a disordered 3D potential created by a blue-detuned speckle with scaled strength $V_0 = 0.5E_\sigma$. For a given energy, we compute the localization length λ_M of a long bar-shaped grid with square section $M \times M$. Each curve is computed for a single M value and shows λ_M/M vs. energy. The various curves cross at the position of the mobility edge. The main plot includes curves from $M = 35$ (less steep, black curve) to $M = 80$ (steepest magenta curve), that suggest a mobility edge around $-0.18E_\sigma$. When only the largest M values are kept – in the inset – a better estimate $E_c = -0.173E_\sigma$ is obtained.

speckle patterns is challenging because the spatial correlations of the potential requires very dense grids, increasing drastically the computational effort. Our starting point is to spatially discretize the Schrödinger equation on a cubic grid with step Δ: the Laplace operator is replaced by a 7 points sum corresponding to an effective hopping rate $J = \hbar^2/(2m\Delta^2)$. The disordered potential at each site is generated by properly convoluting a δ-correlated random sequence in order to reproduce both the on-site potential distribution $P(V)$ and the desired correlation function [23, 26], see Supplemental Material. We first consider the case of a blue speckle, whose distribution is given by Eq. (1). Following [17–19], we chose the simplest case of a speckle created by a statistically isotropic 3D illumination, with correlation function:

$$\langle V(\mathbf{r}')V(\mathbf{r}'+\mathbf{r})\rangle = V_0^2 C(r/\sigma) \qquad (2)$$

where $C(r) = (\sin r/r)^2$ and σ is the characteristic correlation length. Notice that this is different from the scale-free disorder case investigated in [27]. The associated "correlation" energy sets the important energy scale:

$$E_\sigma = \frac{\hbar^2}{m\sigma^2} \qquad (3)$$

where m is the mass of the atom. In the following we measure all energies in units of E_σ. Varying V_0/E_σ can be equivalenty viewed as varying the disorder strength V_0 at fixed σ or the correlation length σ at fixed V_0.

The discretization step must be chosen sufficiently small to resolve the details of the disordered potential and the oscillations of the wavefunction, that is smaller than σ and the de Broglie wavelength, which are similar when V_0 and E are of the order of unity. We have thus chosen a discretization step $\Delta = 0.2\pi\sigma$. We have carefully checked that, up to $V_0 = 1$, the discretization error on the determination of the mobility edge is smaller than 0.005.

The transfer matrix method is used to recursively compute the total transmission of a bar-shaped grid with length L and square transverse section $M \times M$, with $M \ll L$. This system can be viewed as quasi-1D and is thus Anderson localized: its total transmission decays like $\exp(-2L/\lambda_M)$ where λ_M is the quasi-1D localization length in units of the lattice spacing. In practice, the log of the total transmission is a self-averaging quantity which can be safely computed, together with error bars, by using either very long bars or smaller ones but averaging over many independent realizations of the disorder. Periodic boundary conditions are used in the transverse directions to reduce finite-size effects.

λ_M depends on M, on the energy and on the disorder strength. Figure 1 shows the ratio λ_M/M as a function of energy, for various M values, at a fixed disorder strength $V_0 = 0.5$. At low energy, in the localized regime, λ_M/M decreases with M and eventually behaves like λ_∞/M, with $\lambda_\infty = \lim_{M\to\infty} \lambda_M$ the 3D localization length in units of Δ. In contrast, at high energy, λ_M/M increases with M, a signature of the diffusive regime. At the mobility edge, λ_M/M is a constant Λ_c of order unity, meaning that the quasi-1D localization length is comparable to the transverse size of the system, a signature of marginal 3D localization. Thus, the mobility edge can be obtained by looking at the point where all curves cross in Fig. 1. For small M, finite-size effects make the crossing not perfect: looking at only the lowest M, one could get the false impression that the crossing takes place at $E = -0.18$, while the highest M values (inset) show that the true crossing is at $E = -0.173 \pm 0.002$. Reaching such a high precision in the determination of the mobility edge requires massive computing resources: transverse system size up to $M = 80$, longitudinal size of the bar up to 1 million sites. Altogether, data shown in Fig. 1 required 200 000 hours of computation on a supercomputer with slightly more than 10^{19} arithmetic operations.

Finite-size scaling is a technique making it possible to go beyond the visual detection of the crossing, pinpointing more accurately the position of the mobility edge as well as the critical exponent of the Anderson transition. The drift of the crossing point in Fig. 1 is due to the presence of damped oscillations in λ_M as M increases. These oscillations, which are absent in the Anderson model with uncorrelated disorder [25], are probably related to the tail of the correlation function $C(r)$ for $r \approx M\Delta$ and can be hardly incorporated in standard finite-size scaling techniques [25] as "irrelevant variables". We have used this technique, retaining only the data with $M \geq 50$, to confirm the position of the

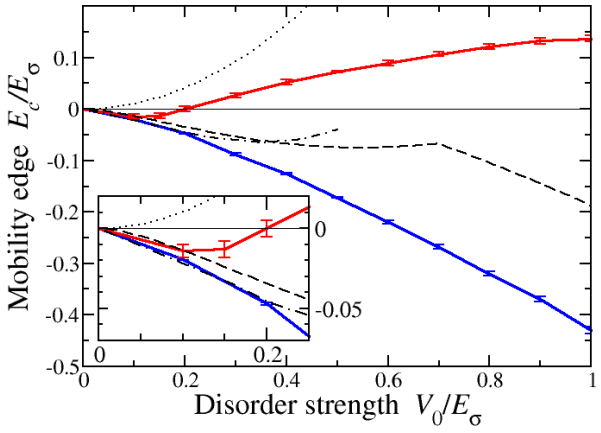

FIG. 2: (color online) Mobility edge separating localized atoms at low energy from diffusive atoms at high energy for cold atoms in a disordered 3D speckle potential (energies in units of the correlation energy, Eq. (3)). The solid lines (lower, blue curve and upper, red curve) correspond respectively to blue and red detuned speckles. While the former mobility edge lies always below the average potential (shown by the horizontal thin line), the latter becomes positive as the potential strength increases (see zoom of the small V_0 region in the inset). The dotted line shows the prediction of the naive self-consistent theory of localization [17]. The dashed [19] and dash-dotted [18] lines are the predictions of improved self-consistent theories incorporating the real part of the self-energy which nevertheless lie rather far from the exact numerical results and do not describe the large difference between blue and red speckles.

Correlation function $C(r)$, eq. (2)	Blue-detuned mobility edge	Red-detuned mobility edge
$[\sin r/r]^2$	-0.172(2)	0.073(2)
$\exp(-r^2/2)$	-0.181(4)	0.054(4)
$\left[3(\sin r/r-\cos r)/r^2\right]^2$	-0.175(5)	0.053(8)

TABLE I: Mobility edge for various disordered speckle potentials, all calculated for $V_0 = 0.5E_\sigma$. The various potentials correspond to different spatial correlation functions, adjusted to have the same width at half-maximum. The mobility edge is computed both for the blue-detuned (positive detuning) and the red-detuned (negative detuning) cases. The digit in parenthesis is the uncertainty on the last digit. The most important factor is the sign of the detuning, while the precise form of the spatial correlation function has only a small effect on the position of the mobility edge.

mobility edge at $E_c = -0.172 \pm 0.0015$, with a critical $\Lambda_c = \lim_{M\to\infty} \lambda_M/M = 0.54 \pm 0.03$ and $\nu = 1.6 \pm 0.2$. These results are less accurate but compatible with the values $\Lambda_c = 0.5765 \pm 0.001$ and $\nu = 1.571 \pm 0.008$ obtained for the Anderson model [25]. Details of the calculation are given in the Supplemental Material, together with a thorough analysis of the single parameter scaling.

We repeat the same calculation for various values of the potential strength. To save computer resources, we use smaller system sizes, producing larger finite size effects, thus slightly larger error bars on the position of the mobility edge, but always smaller than $0.01E_\sigma$. The obtained results for the blue speckle are shown in Fig. 2 by the blue solid line. The mobility edge is negative for all disorder strength V_0; in other words, the mobility edge always lies *below* the average potential.

We also perform analogous calculations for a red speckle, but keeping the spatial correlation function of the disorder, Eq. (2), unchanged. This is shown in Fig. 2 by the red solid line. For small disorder strengths, the mobility edges of red and blue speckles are both negative and very close to each other. In this deep "quantum" regime, the de Broglie wavelength around the mobility edge is larger than σ: the quantum particle thus averages the local potential fluctuations, and is less sensitive to the skewness of the potential distribution. For stronger disorder $V_0 \gtrsim 0.2$, the effect of the asymmetric potential is more important, the mobility edge of the red speckle becomes positive (as clearly shown in the figure inset, despite rather large error bars) and lies well above the blue one. Significant blue/red differences in localization properties have already been observed in the 1D case [28, 29].

We now compare our precise numerical results with the three available theoretical estimates based on different implementations of the SCTL. These are shown in Fig. 2 by the dotted [17], the dash-dotted [18] and the dashed [19] lines. Despite the SCTL being an approximate theory, it turned out to be quite good for simple models such as the Anderson model [30]. The SCTL was naively applied to speckles in [17] assuming that the spectral function and the density of states are unaffected by the disorder. The prediction of this (on-shell) approximation is that the mobility edge is always positive, see Fig. 2, and is obviously rather bad.

A simple attempt to cure this problem is to incorporate in the SCTL the real part of the self-energy, which shifts the effective lower bound of the spectrum to negative energies [34]. Two variants of this simple idea have been used [18, 19], predicting that the mobility edge of the blue speckle is actually negative. However we see in Fig. 2 that these theories become rapidly inaccurate as the disorder strength increases. First, they significantly overestimate the mobility edge. Second, in these approaches, the scattering amplitude is still evaluated at the lowest order in the Born approximation, making the mobility edge dependent only on the correlation function, Eq. (2), but not on the potential distribution, Eq. (1). As a consequence the SCTL predicts *identical* mobility edges for blue and red speckles, which is clearly incorrect. This is not surprising, as the SCTL is not aimed at producing quantitative results beyond the simplest (Gaussian) disorder models.

For further investigation, we use different models of disordered potentials. Table I shows the mobility edges at $V_0 = 0.5$, for red and blue speckles, and various isotropic

Correlation function $C(r)$	Mobility edge
$[\sin r/r]^2$	-0.135(5)
$\exp(-r^2/2)$	-0.124(4)

TABLE II: Mobility edge for Gaussian distributed disordered potentials, calculated for $V_0 = 0.5 E_\sigma$, and two different spatial correlation functions. The mobility edge is between the blue and red results in table I, confirming that the potential distribution is the important factor. Conversely, the precise form of the spatial correlation function has only a small effect.

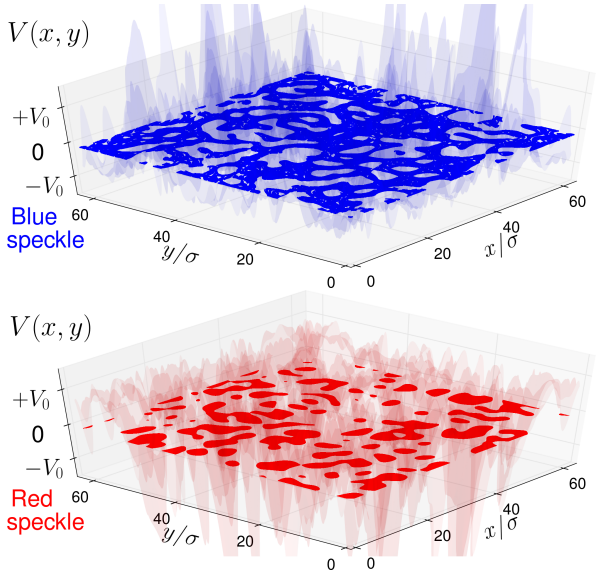

FIG. 3: (color online) Planar cuts in color: classically allowed regions in a transverse section of the grid at energy $-0.15V_0$ (transparent regions are classically forbidden). The allowed region is well connected for the blue speckle and disconnected for the red speckle.

correlation functions $C(r)$ (the third one was adopted in Refs.[31, 32]). In order to make the comparison meaningful, we have adjusted the parameter σ for the potential correlation function to reproduce the same width at half-maximum in the 3 cases, keeping the same strength V_0 of the potential. The mobility edges are almost identical for the 3 blue speckles, around -0.175, and almost identical for the 3 red speckles, around +0.06. This proves that the essential ingredient which determines the mobility edge is the distribution $P(V)$ of disorder strength, and more specifically the fact that the distribution, eq. (1), is very asymmetric. For a blue-detuned speckle, there is a strict lower bound at $-V_0$ (corresponding to the nodes of the speckle) and a long tail towards high V (bright spots of the speckle). There is thus a large probability to find the potential between $-V_0$ and 0. For a red detuned speckle, the potential is upside-down, so that the largest probability is to have the potential between 0 and $+V_0$ and a long tail towards negative V (in both cases, the average potential is 0).

Figure 3 shows the classically available regions on a transverse section of the grid, $V(x, y, z{=}z_0) < E$, for blue and red speckles at the same energy $E = -0.15V_0$, roughly half-way between the two mobility edges. The blue region is strongly connected – which favors delocalization – while the red region is composed of disconnected islands. This percolation argument is mostly valid in the semiclassical limit where $V_0 \gg E_\sigma$, but it already gives the qualitative trend at low V_0 where tunneling plays an important role [33].

The details of the potential correlation function just give rise to small variations of the mobility edge. At the mobility edge, the disorder is so strong that all orders of the Born expansion contribute to the transport properties, smoothing out all details. For example, the kink around $V_0 = 0.7$ in the dashed line of Fig. (2), due to the specificity of the potential correlation function [19], is no longer visible in the "exact" numerical results.

For a symmetric Gaussian distribution of potential $P(V){=}\exp(-V^2/2V_0^2)/\sqrt{2\pi V_0^2}$, the mobility edge, shown in table II, is similar for various correlation functions, around -0.13, but significantly different from the blue and red speckles, although the current implementation of the SCTL gives exactly the same value for the three distributions, around -0.074.

The SCTL does not make accurate quantitative predictions because it uses the lowest order in the Born approximation. As shown in [33], it already does not correctly predict the density of states. The large red-blue difference unambiguously demonstrates that odd powers of V_0 (absent for a Gaussian distribution) play a major role. Even when such terms are absent, the SCTL is not very accurate. We think that inclusion of higher order terms – even approximately – is a necessary step to make these theories more quantitative.

To summarize, we have shown that it is possible to numerically compute the mobility edge for cold atoms exposed to a disordered potential created by a 3D optical speckle. The calculation is quasi-exact (limited only by computer resources) and its accuracy largely sufficient for comparison with experimental results. The mobility edge for a blue-detuned speckle is significantly lower than predicted by the self-consistent theory of localization. We attribute the difference to the peculiar potential distribution of the speckle, while the spatial correlation function defines the characteristic energy scale E_σ but seems otherwise to play a rather minor role. While we have used for simplicity an isotropic disorder correlation function, the method can be extended to the more anisotropic configurations used in the experiments. In the view of the present results, it seems likely that the actual mobility edge lies somewhat lower than measured in the experiments using blue-detuned speckles [14–16]. This problem is currently under investigation.

We thank N. Cherroret, C. Müller, B. Shapiro and S. Pilati for useful discussions. This work was granted

access to the HPC resources of TGCC under the allocation 2013-056089 made by GENCI (Grand Equipement National de Calcul Intensif) and to the HPC resources of The Institute for scientific Computing and Simulation financed by Region Ile de France and the project Equip@Meso (reference ANR-10-EQPX- 29-01).

[1] P. W. Anderson, Phys. Rev. **109**, 1492 (1958).
[2] P. A. Lee and T. V. Ramakrishnan, Rev. Mod. Phys. **57**, 287 (1985).
[3] D. S. Wiersma, P. Bartolini, A. Lagendijk, and R. Righini, Nature (London) **390**, 671 (1997).
[4] M. Störzer, P. Gross, C. M. Aegerter, and G. Maret, Phys. Rev. Lett. **96**, 063904 (2006).
[5] T. Schwartz, G. Bartal, S. Fishman, and B. Segev, Nature (London) **446**, 52 (2007).
[6] Y. Lahini, A. Avidan, F. Pozzi, M. Sorel, R. Morandotti, D. N. Christodoulides, and Y. Silberberg, Phys. Rev. Lett. **100**, 013906 (2008).
[7] H. Hu, A. Strybulevych, J. H. Page, S. E. Skipetrov, and B. A. van Tiggelen, Nat. Phys. **4**, 945 (2008).
[8] A. A. Chabanov, M. Stoytchev, and A. Z. Genack, Nature (London) **404**, 850 (2000).
[9] J. Billy, V. Josse, Z. Zuo, A. Bernard, B. Hambrecht, P. Lugan, D. Clément, L. Sanchez-Palencia, P. Bouyer, and A. Aspect, Nature (London) **453**, 891 (2008).
[10] G. Roati, C. d'Errico, L. Fallani, M. Fattori, C. Fort, M. Zaccanti, G. Modugno, M. Modugno, and M. Inguscio, Nature (London) **453**, 895 (2008).
[11] F. L. Moore, J. C. Robinson, C. F. Bharucha, B. Sundaram, and M. G. Raizen, Phys. Rev. Lett. **75**, 4598 (1995).
[12] J. Chabé, G. Lemarié, B. Grémaud, D. Delande, P. Szriftgiser, and J. C. Garreau, Phys. Rev. Lett. **101**, 255702 (2008).
[13] M. Lopez, J.-F. Clément, P. Szriftgiser, J. C. Garreau, and D. Delande, Phys. Rev. Lett. **108**, 095701 (2012).
[14] S. S. Kondov, W. R. McGehee, J. J. Zirbel, and B. DeMarco, Science **334**, 66 (2011).
[15] F. Jendrzejewski, A. Bernard, K. Muller, P. Cheinet, V. Josse, M. Piraud, L. Pezzé, L. Sanchez-Palencia, A. Aspect, and P. Bouyer, Nat. Phys. **8**, 398 (2012).
[16] G. Semeghini, M. Landini, P. Castilho, S. Roy, G. Spagnolli, A. Trenkwalder, M. Fattori, M. Inguscio, and G. Modugno (2014), arXiv:1404.3528 [cond-mat].
[17] R. Kuhn, O. Sigwarth, C. Miniatura, D. Delande, and C. Müller, New J. Phys. **9**, 161 (2007).
[18] A. Yedjour and B. A. Tiggelen, Eur. Phys. J. D **59**, 249 (2010).
[19] M. Piraud, L. Pezzé, and L. Sanchez-Palencia, New Journal of Physics **15**, 075007 (2013).
[20] D. Vollhardt and P. Wölfle, in *Electronic Phase Transitions*, edited by Hanke, W. and Kopaev Yu. V. (Elsevier, 1992), pp. 1–78.
[21] M. Piraud, L. Pezzé, and L. Sanchez-Palencia, EPL (Europhysics Letters) **99**, 50003 (2012).
[22] R. C. Kuhn, C. Miniatura, D. Delande, O. Sigwarth, and C. A. Müller, Phys. Rev. Lett. **95**, 250403 (2005).
[23] J. Goodman, *Speckle Phenomena in Optics: Theory and Applications* (Roberts & Company Publishers, Dover, Englewood, Colorado, USA, 2007).
[24] A. McKinnon and B. Kramer, Z. Phys. B **53**, 1 (1983).
[25] K. Slevin and T. Ohtsuki, New Journal of Physics **16**, 015012 (2014).
[26] R. Kuhn, Ph.D. thesis, Bayreuth and Nice Universities (2007).
[27] M. Ndawana, R. Roemer, and M. Schreiber, Europhys. Lett. **68**, 678 (2004).
[28] E. Gurevich and O. Kenneth, Phys. Rev. A **79**, 063617 (2009).
[29] P. Lugan, A. Aspect, L. Sanchez-Palencia, D. Delande, B. Grémaud, C. A. Müller, and C. Miniatura, Phys. Rev. A **80**, 023605 (2009).
[30] J. Kroha, T. Kopp, and P. Wölfle, Phys. Rev. B **41**, 888 (1990).
[31] S. Pilati, S. Giorgini, and N. Prokof'ev, Phys. Rev. Lett. **102**, 150402 (2009).
[32] S. Pilati, S. Giorgini, M. Modugno, and N. Prokof'ev, New J. Phys. **12**, 073003 (2010).
[33] B. Shapiro, J. Phys. A **45**, 143001 (2012).
[34] For a blue speckle, there is a strict lower bound $-V_0$ for the energy spectrum, but the density of states is vanishingly small just above $-V_0$. For a red speckle, the energy spectrum is unbounded.

arXiv:1403.3821v2 [cond-mat.quant-gas] 17 Feb 2015

Supplemental material for Mobility edge for cold atoms in laser speckle potential

I. Numerical generation of speckle potentials

In a real experiment, the optical speckle potential is created by superimposing plane waves coming from different directions with random phases. The electric field can then be written as:

$$E(\mathbf{r}) = \sum_{\mathbf{k}_i} A_i e^{i\mathbf{k}_i\cdot\mathbf{r}} W(\mathbf{k}_i), \qquad (1)$$

where A_i is a random complex number with unit modulus, representing the random phase of the plane wave with wave vector $\mathbf{k}_i$, and $W(\mathbf{k}_i)$ is the corresponding weight.

If a large number of uncorrelated plane waves is used, as a consequence of the central limit theorem, the real and the imaginary parts of the electric field at a given point are uncorrelated and follow a Gaussian distribution [**?** **?**]. The optical potential felt by the atom is the modulus square of the electric field, so the on-site potential distribution $P(V)$ follows the Rayleigh law (Eq. (1) of the Letter).

As shown in [**?**], the spatial correlation function of the optical potential is nothing but the squared modulus of the correlation function of the electric field. The latter is directly related to the distribution of the $\mathbf{k}_i$ vectors in the sum, eq. (1). If the $\mathbf{k}_i$ are chosen isotropically on the surface of a sphere, $W(k) = \delta(|\vec{k}| - k_0)$, the field correlation function is a simple sinc function, corresponding to $C(r) = [\sin r/r]^2$ in Eq. (2) of the Letter, with $\sigma = 1/k_0$. If the wave-vectors are chosen with a uniform density inside a sphere, $W(k) = \Theta(k_0 - |\vec{k}|)$, a simple calculation shows that one has: $C(r) = [3(\sin r/r - \cos r)/r^2]^2$. Finally one produces a Gaussian spatial correlation function using $W(k) = \exp(-k^2/2k_0^2)$.

Since the position of the mobility edge is calculated numerically via the transfer-matrix method, we consider a bar-shaped grid with a square transverse section $M \times M$ and a length $L \gg M$. In order to resolve the spatial variations of the potential, the grid step must be small compared to the correlation length of the potential, $\Delta \ll \sigma$.

In order to minimize finite size effects, we chose to use periodic boundary conditions in the two transverse directions. This implies that the disordered potential has the same transverse periodicity. This is of course incompatible with the decay at infinity of the correlation function $C(r)$, Eq. (2) of the Letter. However, converging results are obtained if the transverse size of the system if much larger than the correlation length of the potential, that is $M\Delta \gg \sigma$. Thus, too small values of M must be excluded (in practice, we use at least $M = 30$, that is $M\Delta = 6\pi\sigma$) which explains why the calculation requires large computer resources.

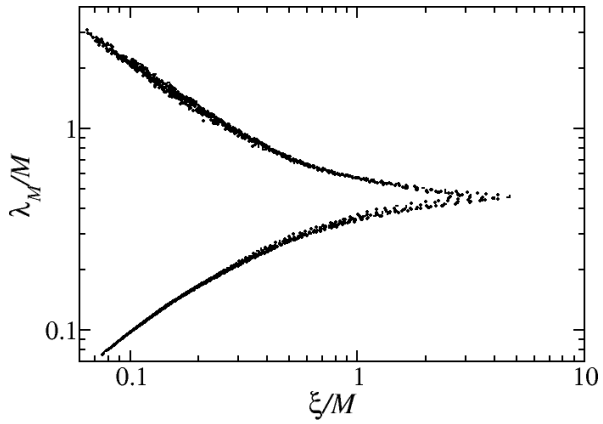

FIG. 1: Scaling function numerically obtained for cold atoms in a disordered 3D blue-detuned speckle potential with strength $V_0 = 0.5E_\sigma$. Data for 201 values of the energy in the range [-0.27,-0.07] and 6 transverse system sizes ($M = 30, 35, 40, 45, 50, 55$) collapse on a unique two-valued scaling function. The lower (resp. upper) branch corresponds to the localized (resp. diffusive) side of the transition; the tip is associated with the divergence of the localization length $\xi(E)$ at the critical point.

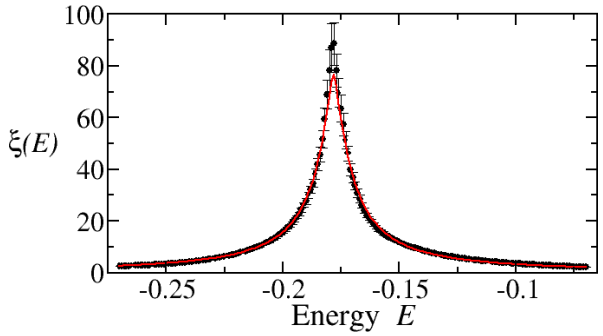

FIG. 2: Localization (resp. correlation) length $\xi(E)$ on the localized (resp. diffusive) side of the metal insulator Anderson transition for cold atoms in a disordered 3D blue-detuned speckle potential with strength $V_0 = 0.5E_\sigma$ (same data than in figure 1). The algebraic divergence near the critical energy $E_c \approx -0.178$ is a characteristic feature of the Anderson transition. The points with error bars are the numerical results and the solid red curve the fit using an algebraic dependence with a cut-off, Eq. (3).

II. Finite-size scaling

Test of one-parameter scaling. As a test of the one-parameter scaling properties of the observed Anderson transition, we used the original finite-size approach described in [**?**]. For this purpose, we gather the quasi-1D localization length λ_M determined for various values of M and of the energy E (at fixed disorder strength).

The one-parameter scaling hypothesis is that there is a unique scaling function $\mathcal{F}$ – or rather a function with two branches – such that:

$$\frac{\lambda_M(E)}{M} = \mathcal{F}\left(\frac{\xi(E)}{M}\right), \tag{2}$$

where $\xi(E)$ is a fitted characteristic length proportional to the localization length in the localized regime and to the inverse of the diffusion constant in the diffusive regime.

Figure 1 shows the scaling function obtained for $V_0 = 0.5$. Since no assumption is made concerning the specific form of the scaling function $\mathcal{F}(x)$, we have used hundreds energy values and, consequently, relatively small systems sizes, $M \leq 55$. The lower (resp. upper) branch is the localized (resp. diffusive) side of the Anderson transition, and the tip on the right side of the figure shows the divergence of the localization length $\xi(E)$ near the critical point.

Figure 2 shows $\xi(E)$. Because the system is finite, it cannot display an infinite divergence. In order to take into account the unavoidable existence of cut-offs, we fit the results with the following formula:

$$\xi(E) = \frac{\alpha}{\beta + |E - E_c|^\nu} \tag{3}$$

where E_c is the mobility edge, ν the critical exponent, α a simple multiplicative factor and β a cut-off.

The fit, shown in Fig 2, is good, although there are clearly deviations in the tails, which is not surprizing as Eq. (2) is expected to be valid only in the very vicinity of the critical point. From the data of Fig.s 1 and 2, we extract $E_c = -0.178$, $\Lambda_c = 0.46$ and $\nu = 1.4$. These values are not very accurate, being affected by strong finite-size corrections, drifting the crossing point towards -0.18, as shown in Fig.1 of the Letter.

Scaling ansatz. More accurate results can be obtained focusing exclusively on large system sizes, for which damped oscillations in λ_M are less important. We thus apply the finite-size scaling ansatz to the numerical data shown in Fig.1 of the Letter with $M \geq 50$ following the procedure outlined in Ref. [**?**].

Taking into account the possible existence of irrelevant operators, the ratio λ_M/M can be written in terms of a new scaling function $\tilde{\mathcal{F}}$ as

$$\frac{\lambda_M(E)}{M} = \tilde{\mathcal{F}}(\phi_1, \phi_2), \tag{4}$$

where the arguments ϕ_1 and ϕ_2 correspond, respectively, to relevant and irrelevant scaling variables. By setting $\omega = (E - E_c)/E_c$, the latter can be expressed as

$$\phi_1 = u_1(\omega) M^{1/\nu} \quad \phi_2 = u_2(\omega) M^y, \tag{5}$$

where $y < 0$ is the exponent of the (dominant) irrelevant operator. In proximity of the critical point, the functions

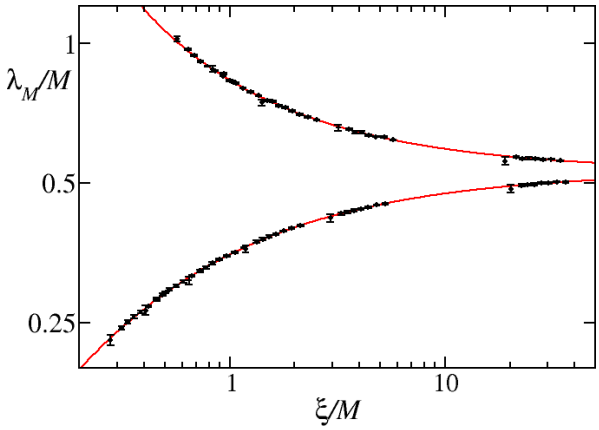

FIG. 3: Same scaling function of Fig.1 but this time obtained using the numerical data in Fig.1 of the Letter with $50 \leq M \leq 90$ and the Taylor expansion of the ansatz. We obtain $E_c = -0.172 \pm 0.0015$, $\Lambda_c = 0.54 \pm 0.03$ and $\nu = 1.6 \pm 0.2.$, compatible with the values $\Lambda_c = 0.576$ and $\nu = 1.57$ found for the 3D Anderson model at zero energy [**?**]. The error bars are comparable to the size of the symbols, except for $M = 90$ (most left point in each series) where there are larger because of less configuration averaging. Altogether, the quality of the fit is satisfactory with a χ^2 per degree of freedom equal to 1.63.

$u_i(\omega)$ are Taylor-expanded up to the order m_i:

$$u_i(\omega) = \sum_{j=0}^{m_i} b_{i,j}\omega^j, \tag{6}$$

where by construction $b_{1,0} = 0$. Next the scaling function $\tilde{\mathcal{F}}(\phi_1, \phi_2)$ is also Taylor-expanded up to orders n_1 and n_2, respectively, yielding

$$\tilde{\mathcal{F}}(\phi_1, \phi_2) = \sum_{j_1=0}^{n_1} \sum_{j_2=0}^{n_2} a_{j_1,j_2} \phi_1^{j_1} \phi_2^{j_2}. \tag{7}$$

To avoid ambiguity in the fitting model we need to set $a_{1,0} = a_{0,1} = 1$ [**?**].

We have fitted our reduced data set using Eqs (4-7). A key point is the choice of the parameters (n_i, m_i). Following [**?**], we choose these parameters just sufficiently large to ensure the fit to be satisfactory, that is with a χ^2 per degree of freedom of the order of unity. Because of (damped) oscillatory behavior with increasing M – not taken into account in the algebraic irrelevant variables – some deviation from the best fit remains, but is typically limited to a χ^2 per degree of freedom in the range from 1 to 4. With $n_1 = m_1 = 2$ and $n_2 = 1, m_2 = 0$, we obtain $E_c = -0.172 \pm 0.0015$, $\Lambda_c = 0.54 \pm 0.03$ and $\nu = 1.6 \pm 0.2$. Similar results are obtained when the degrees parameters (n_i, m_i) are varied.

The obtained results are compatible with the values $\Lambda_c = 0.5765 \pm 0.001$ and $\nu = 1.571 \pm 0.008$ found [**?**] for the 3D Anderson model at zero energy. It is not clear

to us whether exactly the same value of Λ_c should be obtained: indeed, the Anderson model has an anisotropic dispersion relation in the absence of disorder, especially near the band center where the mobility edge is usually studied. This could in principle affect the value of Λ_c.

The more accurate scaling function is then shown in Fig. 3 where we made use of the relation $\xi(E) = |u_1(\omega)|^{-\nu}$. No siginificant deviation of the data from the fit is visible.